Novel Multiform Morphologies of Hydroxyapatite: Synthesis and Growth Mechanism

Article *in* Applied Surface Science · November 2015

DOI: 10.1016/j.apsusc.2015.11.123

Applied Surface Science 361 (2016) 25–32

Contents lists available at ScienceDirect

Applied Surface Science

journal homepage: www.elsevier.com/locate/apsusc

Novel multiform morphologies of hydroxyapatite: Synthesis and growth mechanism

I. Reeta Mary [a,b], S. Sonia [a], S. Viji [a], D. Mangalaraj [a], C. Viswanathan [a], N. Ponpandian [a,*]

[a] Department of Nanoscience and Technology, Bharathiar University, Coimbatore 641046, India
[b] Department of Physics, Government Arts College, Coimbatore 641018, India

ARTICLE INFO

Article history:
Received 6 September 2015
Received in revised form 9 November 2015
Accepted 12 November 2015
Available online 18 November 2015

Keywords:
Nanobiomaterials
Morphology dependence
Electron microscopy
Microstructures

ABSTRACT

Morphological evolution of materials becomes a prodigious challenge due to their key role in defining their functional properties and desired applications. Herein, we report the synthesis of hydroxyapatite (HAp) microstructures with multiform morphologies, such as spheres, cubes, hexagonal rods and nested bundles constructed from their respective nanoscale building blocks via a simple cost effective hydro/solvothermal method. A possible formation mechanism of diverse morphologies of HAp has been presented. Structural analysis based on X-ray diffraction (XRD) and Fourier transform infrared (FTIR) spectroscopy confirms the purity of the HAp microstructures. The multiform morphologies of HAp were corroborated by using Field emission scanning electron microscope (FESEM).

1. Introduction

The recent development in the research of biomaterials has expanded to micro- and nano-scale which has promoted a big break through on the design of advanced functional materials. At this scale, natural materials show delicate hierarchical organizations, complex structures and combination of these, to realize specific functionalities. These micro- and nano-structures assembled from nanoscale building blocks such as nanorods, nanoplates, nanowires, etc., have incredible variations in their specific surface area, particle and pore size, surface roughness and density. Hence, the surface morphology of nanostructured materials plays a major role in determining their structural, optical and surface properties. Accordingly, they can be used in various fields such as photocatalysts, sensors, energy devices, anticancer agents, adsorbents, drug delivery systems etc. [1–4]. For instance, mesoporous Fe_3O_4 nano/micro spheres can be used as drug carriers and MRI contrast agents [5]; micro cubes and nano plates structures of bismuth ferrite show considerable performance during liquefied petroleum, carbon dioxide and ammonium gas sensing applications [6]; ZnO nanodisks and nanorods show sunlight driven photocatalytic activities for methylene blue [7]; $LiMnO_2$ microcubes with interlaced nanoplates is more suitable for application in lithium ion batteries [8]; and the synthesized SnS_2 nanoflakes, nanoflowers and nanoyarns find application in promoting photo-reduction of extremely toxic and lethal Cr(VI) that endorse a new technique for harvesting energy and purification of wastewater [9]. Consequently, synthesizing nanostructured materials with expected morphologies using appropriate and cost effective methods have become a promising issue.

Hydroxyapatite (HAp, $Ca_{10}(PO_4)_6(OH)_2$) is one such best ever known bio ceramic material [10] with wide applications depending on its morphology. Its significance in numerous surface dependent industrial applications such as catalyst support, adsorbents, liquid chromatographic columns, lighting materials, powder carriers, chemical sensors, ion conductors, retardant of cancer cells and drug delivery agent [11–13], etc. are enormous. Though several conventional physical and chemical methods have been used to synthesize nanostructured HAp, hydro/solvothermal synthesis finds its own advantages over the others in controlling their composition, size and morphology under tolerable reaction conditions [14–18]. However, the pH of the precursors, additives, solvents, reaction temperature, reaction time and templates [19–23] influence the structure of HAp significantly. Generally, synthesis of nanostructured hydroxyapatite is carried out either at high reaction temperature above 200 °C or at reaction time 24 h and above, neither the above; post-annealing must be done at high temperatures beyond 300 °C. For example, HAp scaffolds of cauliflower, urchin and porous nanofibrous network grown on titania substrates were synthesized at 240 °C for 4 h [24]; Hydroxyapatite flower-like morphology assembled from nanosheets was synthesized at 200 °C for 24 h [25]; and HAp microspheres were synthesized using droplet

* Corresponding author.
E-mail address: ponpandian@buc.edu.in (N. Ponpandian).

http://dx.doi.org/10.1016/j.apsusc.2015.11.123
0169-4332/

generator device, sintered at 1100 °C [4]. Hence the present work was focused on the evolution of novel multiform morphologies of hydroxyapatite microstructures using mild synthetic conditions.

Herein, we report the synthesis strategies of HAp spheres and hexagonal rods from nanorods, nested bundles from nanosticks and cubes from nanoplates as their nanoscale building blocks by suitably adjusting the additives, pH and solvent of the reaction system at the reaction temperature of 180 °C for 12 h without the necessity of post-annealing treatment. The structural analysis, morphological analysis and the growth mechanism of the so called hydroxyapatite novel microstructures were also dealt in detail. The uniqueness of the present report is the formation of novel multiform morphologies of HAp for the first time under facile reaction medium.

2. Experimental

2.1. Materials

Calcium nitrate tetrahydrate ($Ca(NO_3)_2{\cdot}4H_2O$), di-ammonium hydrogen phosphate ($(NH_4)_2HPO_4$), acetic acid (CH_3COOH), hydrochloric acid (HCl), thiocarbamide (CH_4N_2S), cetyltrimethylammonium bromide (CTAB), urea (NH_2CONH_2), tri-sodium citrate ($Na_3C_6H_5O_7{\cdot}2H_2O$), 30% ammonia solution (NH_4OH), sodium hydroxide (NaOH), potassium hydroxide (KOH), ethylene glycol ($C_2H_6O_2$), ethanol (C_2H_5OH) and di-methyl formamide (DMF) were procured from SDFCL, India. All the above chemical reagents were of analytical grade and used without further purification.

2.2. Synthesis of HAp microstructures

The HAp nanoparticles with multiform morphologies were synthesized by suitably adjusting the additives, pH and solvent of the reaction system under mild hydro/solvothermal reaction conditions.

In a typical HAp microsphere synthesis process, 1 g of CTAB and 0.1 M of calcium nitrate tetrahydrate (CNT) were dissolved in 2:1 ratio of distilled water (DW) and ethylene glycol (EG), and stirred for 30 min in a magnetic stirrer. Also, 0.06 M of di-ammonium hydrogen phosphate (DHP) and 1 g of urea were dissolved in 2:1 ratio of distilled water and ethylene glycol. The pH of this solution was adjusted to 10 using NaOH solution and continuously stirred for 30 min. The prepared phosphate solution was added drop wise to calcium solution and the pH was further adjusted to 5 using hydrochloric acid. Then, 2 g of tri-sodium citrate was added to the resultant solution and stirred for another 30 min to make a homogenous mixture. This homogeneous mixture was further transferred to teflon lined stainless steel autoclave and hydrothermally treated at 180 °C for 12 h and cooled down to room temperature naturally. The final precipitate was washed several times with distilled water to remove the impurities and dried in hot air oven at 100 °C. The reactions were carried out in different solvent systems: (i) distilled water (DW), (ii) DW and ethanol (EtOH), (iii) DW and DMF, and (iv) DW and EG. The HAp spheres were obtained in DW-EG solvent system.

In the synthesis process of cubes, 0.3 M of DHP was dissolved in DW and aqueous ammonia was added till the pH becomes 10. The phosphate solution was added drop wise to the prepared 0.5 M calcium solution and the pH was adjusted to 5 using acetic acid. Thereafter the same procedure for the preparation of spheres was adopted to obtain the cubes. The reaction was repeated by using various pH adjusters for the phosphate solution: (i) potassium hydroxide, (ii) sodium hydroxide and (iii) aqueous ammonia. The HAp cubes were found to be optimized when aqueous ammonia was used to adjust the pH of the phosphate solution.

The hexagonal rods were attained by preparing the HAp nanoparticles using the following process. The 0.3 M DHP solution was prepared in DW and EG in the ratio of 1:2. Also, 0.5 M CNT solution with thiocarbamide (TC-2 g) was prepared in the same ratio of DW and EG. The pH of the phosphate solution was adjusted to 10 by adding NH_4OH and was added drop wise to the calcium solution. The hydrothermal reaction was carried out at 180 °C for 12 h. The product was washed with DW several times and dried at 100 °C. The reactions were carried out by varying the thiocarbamide concentration (i) without TC, (ii) 1 g of TC, (iii) 2 g of TC and (iv) 3 g of TC. The HAp hexagonal rods were optimized with 2 g of thiocarbamide in the reaction.

Nested bundles were prepared with the same procedure like hexagonal rods by replacing the EG with ethanol and also changing the ratio of distilled water and ethanol as 1:0.5. The reactions were carried out by varying the distilled water to ethanol ratio as (i) 1:0, (ii) 1:0.2, (iii) 1:0.5 and (iv) 1:1. The nested bundles were optimized at the ratio of 1:0.5.

The multiform morphologies of the synthesized samples were authenticated by using field emission scanning electron microscope (Quanta 250 FEG). The structure and phase composition of the samples were investigated by X-ray diffraction (PANalytical XPert Pro X-ray diffractometer using Cu $K\alpha_1$ radiation) and Fourier transform infrared spectrometer (Brucker Tensor 27 FTIR Spectrometer).

3. Results and discussion

3.1. Structural evolution of HAp

The XRD pattern for the synthesized HAp microstructures is shown in Fig. 1. The intense diffraction peaks in the XRD patterns indicate the crystalline nature of the synthesized HAp. The XRD peaks at 25.39°, 28.66°, 31.56°, 32.76°, 33.80°, 39.43°, 46.44°, 49.16°, 52.91°, 63.68° and 77.52° corresponding to (0 0 2), (2 1 0), (2 1 1), (3 0 0), (2 0 2), (2 1 2), (4 0 1), (2 1 3), (0 0 4), (3 0 4) and (5 1 3) planes respectively manifested that the obtained samples were of pure form of hydroxyapatite with hexagonal structure. The XRD did not show any other peaks corresponding to secondary phases or intermediate compounds, such as $CaHPO_4{\cdot}2H_2O$ or $Ca_8(HPO_4)_2(PO_4)_4{\cdot}5H_2O$ suggesting that the reaction resulted in the formation of phase pure HAp [26]. All the diffraction peaks were

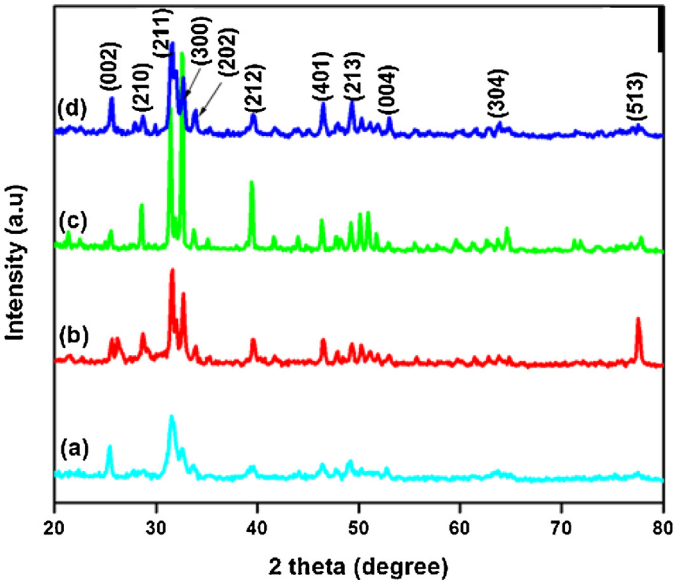

Fig. 1. XRD patterns for (a) spheres, (b) cubes, (c) hexagonal rods and (d) nested bundles.

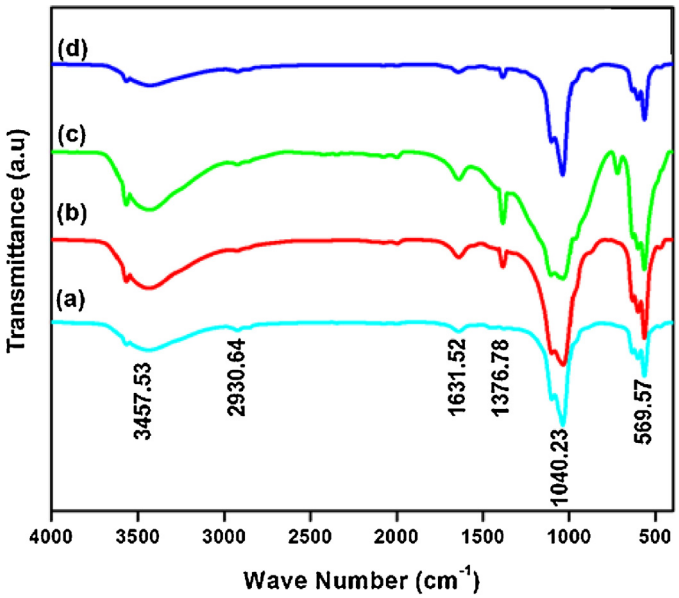

Fig. 2. FTIR spectra for (a) spheres, (b) cubes, (c) hexagonal rods and (d) nested bundles.

unambiguously indexed as a pure hexagonal phase group p63/m, which coincided well with the standard data for HAp (JCPDS #73-0293). The average crystallite sizes of the prepared nanostructured HAp samples estimated by using Scherrer formula were 13, 30, 40 and 21 nm that correspond to spheres, cubes, hexagonal rods and nested bundles respectively. There is no significant change in the lattice parameters ($a = b = 9.4824$ Å and $c = 6.8927$ Å) for the different morphologies of HAp. The XRD results clearly confirms that there is no need of further annealing process which is an additional step for phase, purity and structure transformation of the as-prepared HAp.

The FTIR analysis provides further supporting evidence for the purity of the formed multiform morphologies of HAP microstructures. The FTIR spectra were recorded in the range of 400–4000 cm^{-1} to identify the functional groups present in the prepared samples. Fig. 2 shows the FTIR spectra for different morphologies of HAp microstructures synthesized by hydro/solvothermal process. The intense peaks at 1040 and 569 cm^{-1} are due to PO_4^{3-} stretching and bending modes of the apatite structure [16,27,28]. The broad peak between 2700 and 3800 cm^{-1} can be assigned for the adsorbed water on HAp microstructures [29,30] and the absorption peak at 1631 cm^{-1} was attributed to the bending mode of H_2O [31,32]. The peak at 1376 cm^{-1} might be due to the carbonate ions in the synthesized HAp particles originated from the atmospheric carbon dioxide during the analysis [25,33]. No other peaks in the FTIR spectra clearly confirm the purity of the synthesized HAp microstructures.

3.2. Morphological analysis

The FESEM analysis can provide direct information about the size and typical shapes of the synthesized HAp microstructures.

Fig. 3 shows the series of morphologies prepared by varying the solvent systems to confirm the formation of HAp spheres. In aqueous system, the synthesized nanopowders divulges the starting stage of the formation of agglomerated rod and plate-like morphology undetached from each other as shown in Fig. 3(a), whereas the growth of flake-like morphology was enhanced when distilled water and ethanol were used as shown in Fig. 3(b). The increase in the size of flake-like morphology was noticed in Fig. 3(c) when di-methyl formamide was used as a solvent instead of ethanol. It is evident from Fig. 3(d) that the formation of HAp microspheres with uniform distribution was obtained when distilled water and

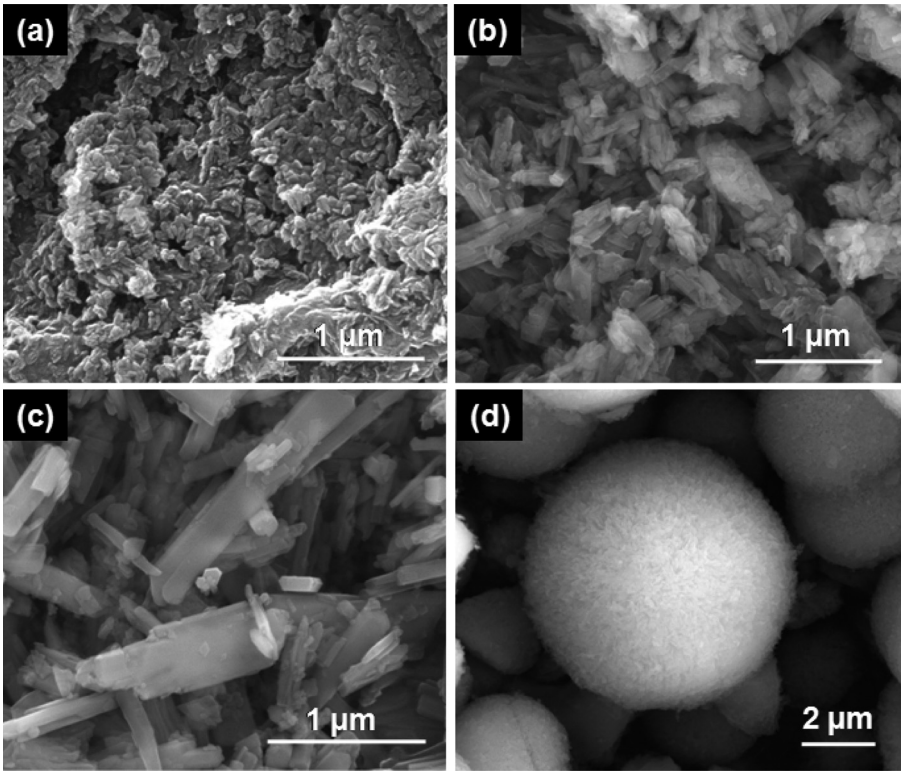

Fig. 3. FESEM images of HAp prepared in different solvents mixed with water (a) pure, (b) ethanol, (c) DMF and (d) EG.

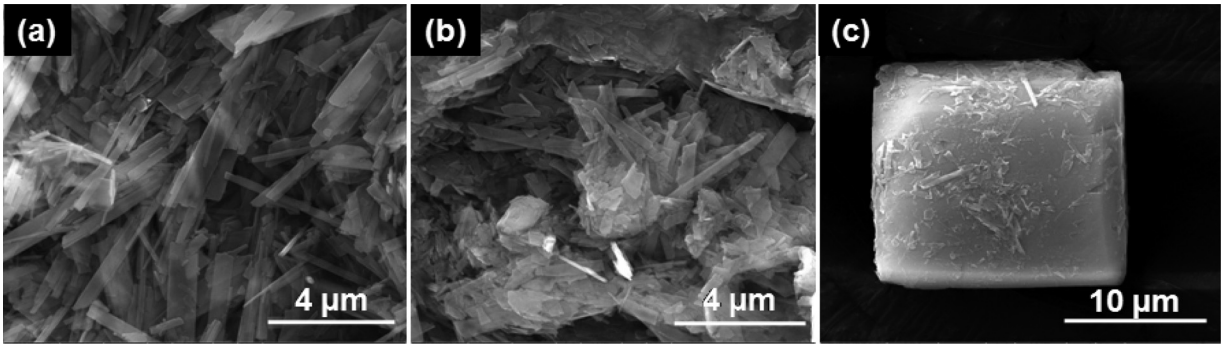

Fig. 4. FESEM images of HAp prepared by various pH adjusters for the Phosphate solution (a) NaOH (b) KOH and (c) NH_4OH (Cubes).

ethylene glycol was used as the solvent. The spheres were constructed from densely packed nanorods as their nanoscale building blocks by self-assembly process.

Fig. 4 shows the morphologies of reaction series during the preparation of nanostructured HAp cubes by using NaOH, KOH and aqueous ammonia as pH adjuster for the phosphate solution. The formation of high aspect ratio nanoplates (HARNPs) were observed when NaOH was used. But the size of the HARNPs was not uniform and the FESEM image reveals that nanoslides and rod-like structures were also formed as in Fig. 4(a). In the presence of KOH, the formed HARNPs tend to aggregate to form a three dimensional nanostructure as shown in Fig. 4(b).

However, it is obvious from Fig. 4(c) that the three dimensional nanostructured cube was formed when ammonium solution was used as the pH adjuster, with nanoplates as nanoscale building blocks.

The series of FESEM images during the formation of hexagonal rods (HRs) by varying the thiocarbamide concentration in the reactions are shown in Fig. 5. Irregular nanoplates were observed during the preparation of HAp in the absence of thiocarbamide (TC) as shown in Fig. 5(a). When 1 g of TC was introduced in the reaction system, the breadth of the plates reduces, leading to nanorods as in Fig. 5(b). Further increase in the concentration of TC to 2 g drastically increases the size of rods resulting in well-defined, crystalline microrods with hexagonal cross-section as shown in Fig. 5(c). Additional increase of TC shows the formation of undefined sphere like morphology as in Fig. 5(d). These results clearly confirm the formation of hexagonal rods when 2 g of TC was used during the synthesis process.

The formation of nested bundles was observed from the FESEM images of Fig. 6. The series of reaction were carried out by varying the amount of ethanol in the solvent system. The formation of nanorods with variation in their size was observed when the solvent was of distilled water alone. As ethanol was introduced in the reaction medium, formation of clusters of nanorods and nested bundles were observed.

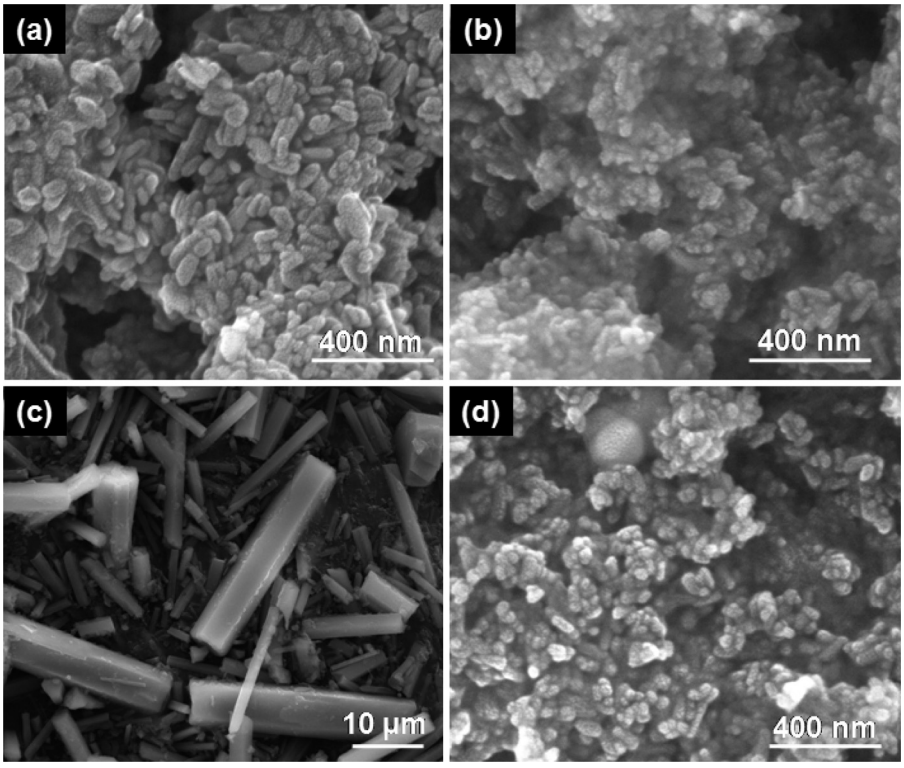

Fig. 5. FESEM images of HAp prepared by varying the TC concentration (a) without TC (b) 1 g of TC (c) 2 g of TC (HRs) and (d) 3 g of TC.

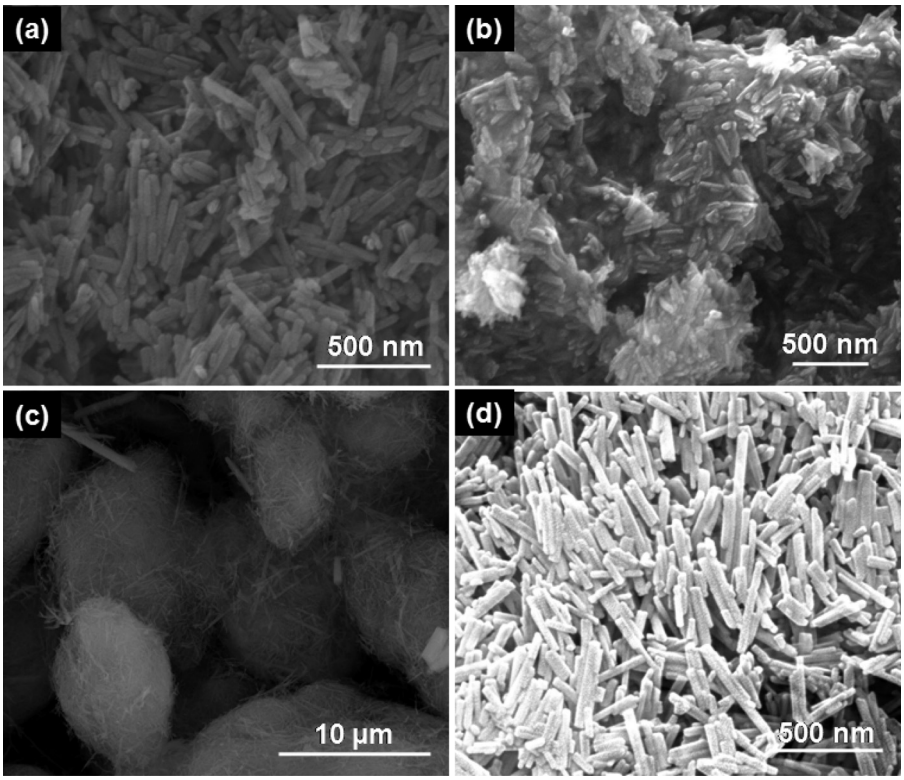

Fig. 6. FESEM images of HAp prepared by varying the DW and EtOH ratio.

Fig. 7 shows the FESEM images for the surface morphologies of HAp microstructures with different magnifications. From these images, it is clear that the HAp microstructures have diverse well-defined shapes. Fig. 7(a–c) shows the FESEM images for the formation of HAp microspheres with the diameter of 7 μm, assembled from densely packed nanorods with a width of 80 nm. Fig. 7(d–f) shows the microcubes with the side length of 12 μm, ripened from nanoplates. These nanoplates have a length and width of 1–1.5 μm and 0.3 μm respectively as shown in the high magnification image. The hexagonal microrods in Fig. 7(g–i) were formed due to Ostwald ripening process. These hexagonal rods have an average length and diameter of 25 and 5 μm respectively. The nested bundles in Fig. 7(j–l) were formed by the self-assembly of nanosticks with the length of 1–2 μm. It was evident that the synthesized HAp microstructures were systematically formed by one and two dimensional nanostructures such as nanorods, nanoplates and nanosticks which act as the nanoscale building blocks as shown in Fig. 7(c, f, l).

3.3. Growth mechanism

The reaction mechanism for the formation of stoichiometric HAp using calcium nitrate and di-ammonium hydrogen phosphate as precursors for Ca^{2+} and PO_4^{3-} respectively is given as follows:

$$6(NH_4)_2HPO_4 + 10Ca(NO_3)_2 + 8NH_4OH \rightarrow Ca_{10}(PO_4)_6(OH)_2 + 20NH_4NO_3 + 6H_2O$$

The growth mechanism of HAp microstructures involves crystallization, Ostwald ripening and self-assembly processes which were supposed to be the specific channels for the formation of different morphologies. The larger particles are grown from primary units by oriented attachment in Ostwald ripening whereas in self-assembly, the adjacent nanoparticles were shared with their common crystallographic orientations [34–37]. Herein, cubes and hexagonal rods were formed from the oriented attachment of nanoplates and nanorods respectively by Ostwald ripening, and the self-organization of nanosticks and nanorods pave the way for the formation of nested bundles and spheres respectively, as shown in Fig. 8.

The growth of nanostructured HAp spheres starts with the formation of micelles. In general, CTAB forms spherical or cylindrical micelles [3] depending on their critical micelle concentration. As cylindrical micelle forms above 23 wt% of CTAB [38], the formed HAp nanorods were due to the same. CTAB-Ca^{2+} rod-like micelles were produced because of the concentration difference between the inside-water phase and the outside-oil phase of the rod-like CTAB micelles where the Ca^{2+} were transferred to the surface of the micelles. When the PO_4^{3-} solution was added to this CTAB-Ca^{2+} solution, HAp clusters were preferentially condensed on the rod-like micelle's surface due to the strong electrostatic interaction between cationic surfactant CTAB and anionic inorganic precursor PO_4^{3-}, since CTAB acts as a strong acid weak base salt [39]. Thus the micelles act as nucleating sites for the growth of HAp crystals. The formed CTAB-HAp complexes then coalesce to form a stable one dimensional nanorod structure [40]. Besides, NH_4OH generated from the hydrolysis of aqueous urea increases the rate of nucleation and growth of nanorods under moderate supersaturation conditions [41]:

$$(NH_2)_2CO + H_2O \rightarrow 2NH_3 + CO_2$$

$$NH_3 + H_2O \rightarrow NH^{4+} + OH^-$$

However, the addition of HCl restrains the growth rate by suppressing the OH^- concentration resulting in short rods. These short

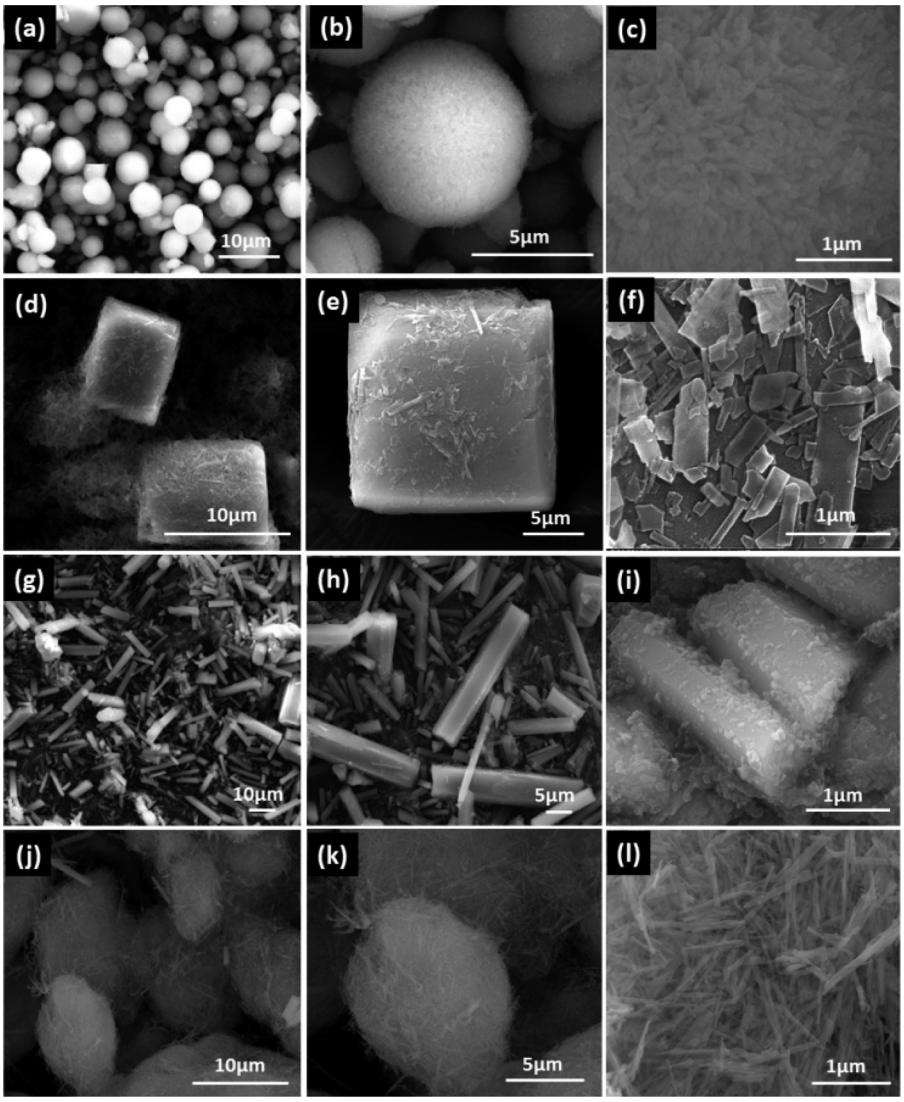

Fig. 7. FESEM images with different magnifications of (a–c) spheres, (d–f) cubes, (g–i) hexagonal rods and (j–l) nested bundles.

rods self-assemble to form spheres in solvothermal environment with the help of EG which was used as a co-solvent. The –COOH and –OH groups of tri-sodium citrate adsorbed on the surface of the self-oriented nanorods prevent the accumulation of microspheres [42] resulting in mono-dispersed HAp spheres.

Generally the growth of HAp in aqueous solution results in a three dimensional structure. The shape was determined by the relative specific surface energies associated with the facets of crystal. The facets of HAp have a preference to adsorb OH^- [43] and results in rod-like morphology. But the increase of OH^- ions on the interface produces a shielding effect due to which the rate of growth was controlled in different facets. The adsorbed OH^- ions were partly neutralized by the addition of acetic acid which boosts the growth of the nuclei in all the facets. However, the hindrance effect of acetic acid inhibits the longitudinal growth which leads to the formation of nanoplates as shown in Fig. 7f. These nanoplates yield well-defined nanostructured cubes through Ostwald ripening process.

The growth of apatite in aqueous solution is a prolonged and slow process resulting in perfect and large crystals. Also, the preferential growth of HAp is along the *c*-axis [44]. Since thiocarbamide is known to promote the growth along a plane [45], the formation of microrods could be due to the bonding interaction between the amine groups and the HAp particles. The hexagonal cross section of the rod might be due to the shape controlling nature of $CS(NH_2)_2$. Ethylene glycol was used as a co-solvent to promote the longitudinal *c*-axis growth of the hexagonal rod leading to a microstructure.

During the growth of nested bundles, the clusters of HAp particles were grown as nanorods during the initial nucleation and growth processes when water is used as a solvent. The polarity [46,47], dielectric constant [48] and viscosity of the solvents influenced the nucleation as well as the preferential direction of the crystal growth [21]. The higher dielectric constant and lower viscosity of water enhances the growth of nanorods to nanosticks, and the aggregation and self-assembly of these nanosticks to form bundles might be due to lower dielectric constant and higher viscosity of ethanol. Here, the double solvent system plays a dynamic role in the formation of nested bundles as they have strong effect on the solubility, reactivity and diffusion behavior of the reactants.

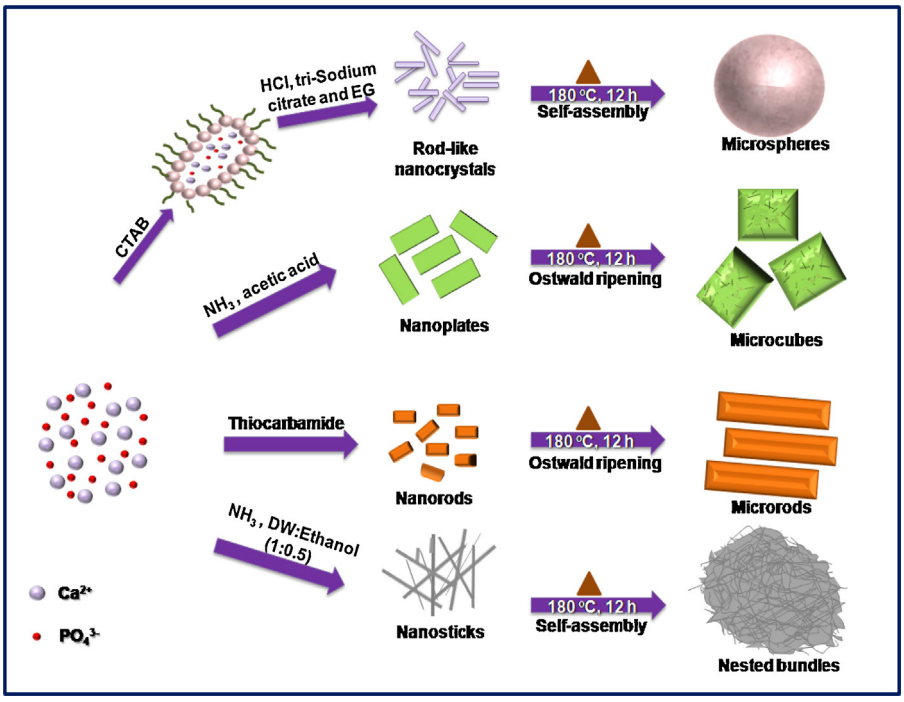

Fig. 8. Schematic illustration of growth processes of HAp microstructures.

4. Conclusion

Novel multiform microstructures of HAp with four different morphologies were successfully synthesized by facile hydro/solvothermal process under mild reaction medium, by varying the preparatory conditions without the stipulation of post-annealing treatment. Structural analysis reveals the phase, purity and crystallinity of the designed HAp microstructures. The distinct and well-aligned microstructures of HAp were confirmed by the morphological analysis. The proposed growth mechanism of the HAp morphologies elucidates the growth of microstructures based on crystallization, Ostwald ripening and self-assembly processes. In conclusion, the morphology of the novel microstructures was controlled by the reactants in the solvent system which acts as promoters/inhibitors for the nucleation and growth processes.

Acknowledgements

The authors would like to thank the DST, Government of India for the FESEM facility through DST-PURSE and financial assistance through DST-FIST program.

References

[1] L. Li, R. Lin, Z. Tong, Q. Feng, Facile synthesis of $SrCO_3$ nanostructures in methanol/water solution without additives, Nanoscale Res. Lett. 7 (2012) 1–5.
[2] W. Wei, G.H. Ma, G. Hu, Y. Di, T. Mcleish, Z.G. Su, Z.Y. Shen, Preparation of hierarchical hollow $CaCO_3$ particles and the application as anticancer drug carrier, J. Am. Chem. Soc. 130 (2008) 15808–15810.
[3] N.C. Sagaya Selvam, J.J. Vijaya, L.J. Kennedy, Effects of morphology and Zr doping on structural, optical, and photocatalytic properties of ZnO nanostructures, Ind. Eng. Chem. Res. 51 (2012) 16333–16345.
[4] A.Y. Pataquiva Mateus, Comparative study of nanohydroxyapatite microspheres for medical applications, J. Biomed. Mater. Res. Part A (2007) 483–493.
[5] S. Xuan, F. Wang, Josie M.Y. Lai, Kathy W.Y. Sham, Yi-Xiang J. Wang, Synthesis of biocompatible, mesoporous Fe_3O_4 nano/microspheres with large surface area for magnetic resonance imaging and therapeutic applications, ACS Appl. Mater. Interfaces 3 (2011) 237–244.
[6] S.D. Waghmare, V.V. Jadhav, S.K. Gore, S.J. Yoon, S.B. Ambade, B.J. Lokhande, Efficient gas sensitivity in mixed bismuth ferrite micro (cubes) and nano (plates) structures, Mater. Res. Bull. 47 (2012) 4169–4173.
[7] S. Kuriakose, B. Satpati, S. Mohapatra, Enhanced photocatalytic activity of Co doped ZnO nanodisks and nanorods prepared by a facile wet chemical method, Phys. Chem. Chem. Phys. 16 (2014) 12741–12749.
[8] H. Xu, J. Sun, L. Gao, Hydrothermal synthesis of $LiMnO_2$ microcubes for lithium ion battery application, Ionics 19 (2013) 63–69.
[9] C. Mondal, M. Ganguly, J. Pal, A. Roy, J. Jana, T. Pal, Morphology controlled synthesis of SnS_2 nanomaterial for promoting photocatalytic reduction of aqueous Cr(VI) under visible light, Langmuir 30 (2014) 4157–4164.
[10] S.V. Dorozhkin, M. Epple, Biological and medical significance of calcium phosphates, Angew. Chem. Int. Ed. Engl. 41 (2002) 3130–3146.
[11] T.G. Kim, B. Park, Synthesis and growth mechanisms of one-dimensional strontium hydroxyapatite nanostructures, Inorg. Chem. 44 (2005) 9895–9901.
[12] Y.J. Wang, J.D. Chen, K. Wei, S.H. Zhang, X.D. Wang, Surfactant-assisted synthesis of hydroxyapatite particles, Mater. Lett. 60 (2006) 3227–3231.
[13] Q.J. He, Z.L. Huang, Controlled growth and kinetics of porous hydroxyapatite spheres by a template-directed method, J. Cryst. Growth 300 (2007) 460–466.
[14] Z. Hai-bin, Z. Ke-chao, L. Zhi-you, H. Su-ping, Z. Yan-zhong, Morphologies of hydroxyapatite nanoparticles adjusted by organic additives in hydrothermal synthesis, J. Cent. South Univ. Technol. 16 (2009) 0871–0875.
[15] K. Ioku, S. Yamauchi, H. Fujimori, S. Goto, M. Yoshimura, Hydrothermal preparation of fibrous apatite and apatite sheet, Solid State Ionics 151 (2002) 147–150.
[16] J. Liu, X. Ye, H. Wang, M. Zhu, B. Wang, H. Yan, The influence of pH and temperature on the morphology of hydroxyapatite synthesized by hydrothermal method, Ceram. Int. 121 (2002) 59–64.
[17] P. Sujaridworakun, F. Koh, T. Fujiwara, D. Pongkao, A. Ahniyaz, M. Yoshimura, Preparation of anatase nanocrystals deposited on hydroxyapatite by hydrothermal treatment, Mater. Sci. Eng. C 25 (2005) 87–91.
[18] M. Yoshimura, P. Sujaridworakun, F. Koh, T. Fujiwara, D. Pongkao, A. Ahniyaz, Hydrothermal conversion of calcite crystals to hydroxyapatite, Mater. Sci. Eng. C 24 (2004) 521–525.
[19] P. Wang, C. Li, H. Gong, X. Jiang, H. Wang, K. Li, Effects of synthesis conditions on the morphology of hydroxyapatite nanoparticles produced by wet chemical process, Powder Technol. 203 (2010) 315–321.
[20] A. Lak, M. Mazloumi, M. Mohajerani, Self-assembly of dandelion-like hydroxyapatite nanostructures via hydrothermal method, J. Am. Ceram. Soci. 91 (2008) 3292–3297.
[21] H. Alobeedallah, J.L. Ellis, R. Rohanizadeh, H. Coster, F. Dehghani, Preparation of nanostructured hydroxyapatite in organic solvents for clinical applications, Trends Biomater. Artif. Organs 25 (2011) 12–19.
[22] S.C. Joachim Loo, Y.E. Siew, F.Y. Shuhui Ho, Chiang Boey, J. Ma, Synthesis and hydrothermal treatment of nanostructured hydroxyapatite of controllable sizes, J. Mater. Sci. Mater. Med. 19 (2008) 1389–1397.
[23] K. Takahiro, S. Hironobu, U. Hidero, Preparation of hollow hydroxyapatite microspheres utilizing poly(divinylbenzene) as a template, J. Ceram. Soc. Jpn. 117 (2009) 340–343.

[24] S. Nayak, B. Satpati, R.K. Shukla, Facile synthesis of nanostructured hydroxyapatite-titania bio-implant scaffolds with different morphologies: their bioactivity and corrosion behavior, J. Mater. Chem. 20 (2010) 4949–4954.
[25] M.G. Ma, Hierarchically nanostructured hydroxyapatite: hydrothermal synthesis, morphology control, growth mechanism, and biological activity, Int. J. Nanomed. 7 (2012) 1781–1791.
[26] G.A. Martinez-Castanon, J.P. Loyola-Rodriguez, N.V. Zavala-Alonso, Preparation and characterization of nanostructured powders of hydroxyapatite, Superficies y Vacio 25 (2012) 101–105.
[27] S. Kannan, A.F. Lemos, J.M.F. Ferreira, Synthesis and mechanical performance of biological-like hydroxyapatites, Chem. Mater. 18 (2006) 2181–2186.
[28] T.A. Kuriakose, S.N. Kalkura, M. Palanichamy, Synthesis of stoichiometric nano crystalline hydroxyapatite by ethanol-based sol-gel technique at low temperature, J. Cryst. Growth 263 (2004) 517–523.
[29] R.N. Panda, M.F. Hsieh, R.J. Chung, T.S. Chin, FTIR, XRD, SEM and solid state NMR investigations of carbonate-containing hydroxyapatite nano-particles synthesized by hydroxide-gel technique, J. Phys. Chem. Solids 64 (2003) 193–199.
[30] V. Jokanovic, D. Izvonar, M. Dramicanin, Hydrothermal synthesis and nanostructure of carbonated calcium hydroxyapatite, J. Mater. Sci. Mater. Med. 17 (2006) 539–546.
[31] A. Balamurugan, J. Michel, J. Faure, Synthesis and structural analysis of sol gel derived stoichiometric monophasic hydroxyapatite, Ceramics-Silikaty 50 (2006) 27–31.
[32] M.G. Ma, Y.J. Zhu, J. Chang, Monetite formed in mixed solvents of water and ethylene glycol and its transformation to hydroxyapatite, J. Phys. Chem. B 110 (2006) 14226–14230.
[33] R. Kumar, K.H. Prakash, P. Cheang, K.A. Khor, Temperature driven morphological changes of chemically precipitated hydroxyapatite nanoparticles, Langmuir 20 (2004) 5196–5200.
[34] H.G. Yang, H.C. Zeng, Nanospheres via Ostwald ripening, J. Phys. Chem. B 108 (2004) 3492–3495.
[35] W.Z. Ostwald, Upper the supposed isomerism of red and yellow mercuric oxide and the upper flchenspannung solid, Phys. Chem. 34 (1900) 495–503.
[36] R.L. Penn, J.F. Banfield, Imperfect oriented attachment: dislocation generation in defect-free nanocrystals, Science 281 (1998) 969–971.
[37] Q. Zhang, S.J. Liu, S.H. Yu, Recent advances in oriented attachment growth and synthesis of functional materials: concept, evidence, mechanism, and its future, J. Mater. Chem. 19 (2009) 191–207.
[38] O.B. David, E.N. Roth, R.Y. Rozen, M. Gottlieb, Rheological investigation of single-walled carbon nanotubes-induced structural ordering in CTAB solutions, Soft Matter 5 (2009) 1925–1930.
[39] Y. Zou, Y. Li, N. Zhanng, Liu, Flower-like CuO synthesized by CTAB-assisted hydrothermal method, Bull. Mater. Sci. 34 (2011) 967–971.
[40] S. Manafi, M.R. Rahimipour, B. Yazdani, S.K. Sadrnezhaad, M.H. Amin, Hydrothermal synthesis of aligned hydroxyapatite nanorods with ultra-high crystallinity, IJE Trans. B: Appl. 21 (2008) 109–116.
[41] I.S. Neira, Y.V. Kolenko, An effective morphology control of hydroxyapatite crystals via hydrothermal synthesis, Cryst. Growth Des. 9 (2009) 466–474.
[42] S. Kuriakose, V. Choudhary, B. Satpati, S. Mohapatra, Enhanced photocatalytic activity of Ag–ZnO hybrid plasmonic nanostructures prepared by a facile wet chemical method, Beilstein J. Nanotechnol. 5 (2014) 639–650.
[43] W.J. Li, E.W. Shi, W.Z. Zhong, Z.W. Yin, Growth mechanism and growth habit of oxide crystals, J. Cryst. Growth 203 (1999) 186–196.
[44] T. Ma, Z. Xia, L. Liao, Effect of reaction systems and surfactant additives on the morphology evolution of hydroxyapatite nanorods obtained via a hydrothermal route, Appl. Surf. Sci. 257 (2011) 4384–4388.
[45] P.B. Khoza, M.J. Moloto, L.M. Sikhwivhilu, The effect of solvents, acetone, water, and ethanol, on the morphological and optical properties of ZnO nanoparticles prepared by microwave, J. Nanotechnol. (2012) 1–6.
[46] X.W. Lou, Y. Wang, C.L. Yuan, J.Y. Lee, L.A. Archer, Template-free synthesis of SnO_2 hollow nanostructures with high lithium storage capacity, Adv. Mater. 18 (2006) 2325–2329.
[47] J.R. Speakman(Edr), G.H. Visser, S. Ward, E. Krol, The isotope dilution method for the evaluation of body composition, in: Body Composition Analysis of Animals – A Handbook of Non-Destructive Methods, 2001, pp. 56–98.
[48] F. Manoli, E. Dalas, Spontaneous precipitation of calcium carbonate in the presence of ethanol, isopropanol and diethylene glycol, J. Cryst. Growth 218 (2000) 359–364.